Synaptic Specializations at Dopamine Release Sites Orchestrate Efficient and Precise Neuromodulatory Signaling

Chandima Bulumulla, Deepika Walpita, Nirmala Iyer, Mark Eddison, Ronak Patel, Damien Alcor, David Ackerman, Abraham G. Beyene*

Janelia Research Campus, Howard Hughes Medical Institute, Ashburn, VA, 20147, United States.

* Corresponding author. Email: beyenea@janelia.hhmi.org

Abstract: Dopamine is a key chemical neuromodulator that plays vital roles in various brain functions. Traditionally, neuromodulators like dopamine are believed to be released in a diffuse manner and are not commonly associated with synaptic structures where pre- and postsynaptic processes are closely aligned. Our findings challenge this conventional view. Using single-bouton optical measurements of dopamine release, we discovered that dopamine is predominantly released from varicosities that are juxtaposed against the processes of their target neurons. Dopamine axons specifically target neurons expressing dopamine receptors, forming synapses to release dopamine. Interestingly, varicosities that were not directly apposed to dopamine receptor-expressing processes or associated with neurons lacking dopamine receptors did not release dopamine, regardless of their vesicle content. The ultrastructure of dopamine release sites share common features of classical synapses. We further show that the dopamine released at these contact sites induces a precise, dopamine-gated biochemical response in the target processes. Our results indicate that dopamine release sites share key characteristics of conventional synapses that enable relatively precise and efficient neuromodulation of their targets.

Introduction: Two types of chemical signaling facilitate interneuronal communication in the brain. The first type, fast synaptic transmission, occurs between precisely coupled synaptic partners, where the activation of ligand-gated ion channels elicits depolarizing or hyperpolarizing electrical responses. The molecular and cellular mechanisms underlying fast synaptic transmission have been extensively studied(*1, 2*). The second type of communication involves neuromodulators, which are released volumetrically and act diffusively on their targets across a broader area(*3*). Although volumetrically released neuromodulators control the efficacy of fast synaptic transmission, and therefore play a critical role in neuronal computation that underlies cognition and behavior(*4, 5*), the precise nature of their release sites is less well understood and remains an active area of research.

Histochemical and electron microscopy studies of dopamine neurons have been instrumental in advancing the concept of volumetric signaling (also known as volume transmission) as a distinct mode of interneuronal communication mediated by neuromodulators(*6-9*). The evidence supporting volumetric signaling includes ultrastructural findings that reveal that the majority (up to 67% in some studies) of dopaminergic varicosities lack clear synaptic juxtapositions in various areas of the cortex and the striatum(*10-13*). Similar observations were made in neurons that release other monoamines and neuropeptides(*14-18*). The presence of extrasynaptically localized dopamine receptors further bolstered the concept of volume transmission, suggesting that a diffuse neuromodulatory tone permeating a defined volume of neuronal tissue may be

sufficient for receptor activation(*19-21*). Furthermore, the inherently slow timescales associated with G-protein coupled receptor (GPCR) signaling suggests a precise juxtaposition between pre- and postsynaptic partners may not be necessary(*3*). Thus, a diverse set of observations established volume transmission as a model for neuromodulator-mediated chemical communication between neurons.

However, recent evidence challenges the traditional view that dopamine neuromodulation is inherently slow and lacks precision. Studies have shown a precise correlation between the firing patterns of dopamine neurons and their rapid modulatory effects on behavior(*22-26*). Ultrastructural examinations have also identified subsets of dopamine axon terminals that form synapses or synapse-like associations with postsynaptic partners(*27-30*). Despite these findings, the functional distinctions between synapse-forming and non-synapse-forming varicosities are not known. Additionally, optical biosensors for dopamine have indicated the presence of release hotspots in the striatum(*31-33*), originating from active zones enriched with some of the same proteins responsible for fast synaptic signaling(*34, 35*). Collectively, these findings suggest that dopamine signaling may be more spatially and temporally regulated than previously thought, necessitating a re-evaluation of the mechanisms underlying dopamine release.

In this study, we used a diverse array of cellular and molecular methodologies, and activity correlated light and electron microscopy to investigate the morphological, ultrastructural, and molecular characteristics of dopamine releasing varicosities, and how these varicosities are organized relative to each other and relative to the processes of putative target neurons. In co-cultures of primary dopamine neurons and cortical neurons or striatal neurons, we observed that dopamine was chiefly released at varicosities that were juxtaposed against dendrites or soma, which represented ~34% of the total varicosities in an axonal arbor. Furthermore, axonal varicosities lacking such juxtaposition or that were apposed against processes that did not express dopamine receptors did not release dopamine, irrespective of their vesicle content, emphasizing the indispensability of proximity to appropriate targets for release competency. In cortical co-cultures, release competent dopamine varicosities form pericellular baskets that terminate on the soma and proximal dendrites of dopamine receptor-expressing neurons and, when stimulated, secrete a “corona” of extracellular dopamine that envelop the cell body and major dendrites, and modulate cyclic AMP (cAMP) levels. In brain slices, we confirmed axo-somatic innervations of cortical neurons by dopaminergic axons in the mouse medial prefrontal cortex. Based on evidence presented in this study, we propose that axo-somatic pericellular baskets and synapse forming varicosities that innervate distal dendrites are specialized structures that facilitate temporally precise and efficient neuromodulation of their targets. In summary, our results offer new insights into dopamine release sites, challenging the conventional notion that dopamine signaling is predominantly volumetric and imprecise, and thus expanding the modalities of chemical signaling available for neural computation.

Results

Dopamine Release Arise from Varicosities that are Apposed to Neuronal Dendrites and Soma

Our study employs an optical assay called DopaFilm, which is a composite 2-dimensional fluorescent nanomaterial that incorporates optically sensitive dopamine nanosensors on glass coverslips via a simple drop-cast deposition process(*36*). When exposed to dopamine, DopaFilm exhibits a rapid, intensiometric modulation in fluorescence. We derived primary neurons from P1 – P2 pups of slc6a3-cre (DAT-cre) mice that were crossed with Ai9 reporter mice. Consistent with previous reports, this approach expressed tdTomato (tdTom) in dopaminergic neurons with >90% specificity (*37, 38*). When cultured on DopaFilm, tdTom-tagged axonal varicosities that release dopamine elicit quantifiable fluorescence hotspots, which we report as relative changes in fluorescence intensity from baseline ($\Delta F/F$). By cultivating a sparse monolayer of dopamine neurons on DopaFilm-coated coverslips, we captured the complete spatiotemporal profile of dopamine release, including hotspot formation and dissipation, from both evoked and spontaneously active neurons. This approach enabled us to localize dopamine sources with single-bouton resolution across fields of view encompassing individual or multiple neuronal axonal arbors (fig. S1). Subsequently, we conducted post hoc analyses of the same varicosities using immunofluorescence imaging and serial-section transmission electron microscopy (Fig. 1A). This multi-modal approach allowed us to correlate functional activity data with morphological, ultrastructural, and protein expression profiles at single-bouton precision.

We made three key observations while imaging in axonal arbors of dopamine neurons that are co-cultured with either cortical or striatal neurons (Fig. 1). First, we noted that release emanates from a subset of varicosities within the field of view, with considerable segments of dopamine axonal processes remaining inactive (Fig. 1B, fig. S2 – S17). The release active fraction of varicosities varied notably across fields of view (0.34 ± 0.27, Mean$\pm$SD, from n = 17 samples). Second, release-competent varicosities were spatially clustered, resulting in a distinctly inhomogeneous dopamine release profile across the imaging field (Fig. 1B – 1E, fig. S2 – S17). To quantify the inhomogeneity of dopamine release (or clustering of dopamine release sites), we examined the distribution of pairwise distances between *tdTom+* pixels, which represent dopaminergic axonal processes in the imaging field (Fig. 1A). The pairwise-distance distribution function of release competent *tdTom+* pixels, defined as those that overlapped with $\Delta F+$ pixels, displayed a prominent peak at small interpixel distances, which contrasted with the distribution of pairwise distances in inactive *tdTom+* pixels and all *tdTom+* pixels (Fig. 1F, p-value $< 10^{-4}$ on active vs. inactive pixels distribution using two sample Kolmogorov-Smirnov test, KS statistic = 0.769). This analysis was repeated for the nine fields of view presented in fig. S9 – S17 and is summarized in Fig. 1G. These calculations reveal that release-competent *tdTom+* pixels exhibit a clustering with peak pairwise distances occurring at 10.5 ± 7.9 µm (Mean$\pm$SD), representing a characteristic size scale for dopamine release hotspots. In contrast, the pairwise distance distributions of all *tdTom+* pixels or inactive *tdTom+* pixels in a given field of view were broad and lacked distinct features (Fig. 1F – 1G). This analysis suggested a non-arbitrary distribution of release competence in axonal varicosities of dopamine neurons.

Third, we observed that the release-competent varicosities were apposed to soma (Fig. 1D) or dendrites of neurons in the co-culture assay (Fig. 1C, 1E), directing dopamine release toward these putative target processes (fig. S2 – S17). To quantify the proximity of release-active *tdTom+* pixels to neuronal processes, we immunostained for the somatodendritic marker MAP2 and plotted the normalized ΔF value at each *tdTom+* pixel as a function of its nearest distance from a MAP2-positive neuronal process. This analysis unveiled a correlation between the

amplitude of dopamine release at a *tdTom+* pixel and its proximity to MAP2 (Fig. 1H). This finding was repeated across the nine fields of view presented in fig. S9 – S17, and the results are summarized in Fig. S18. This quantification indicated that dopamine release is more vigorous in tdTom process that are co-located with neuronal dendrites and soma.

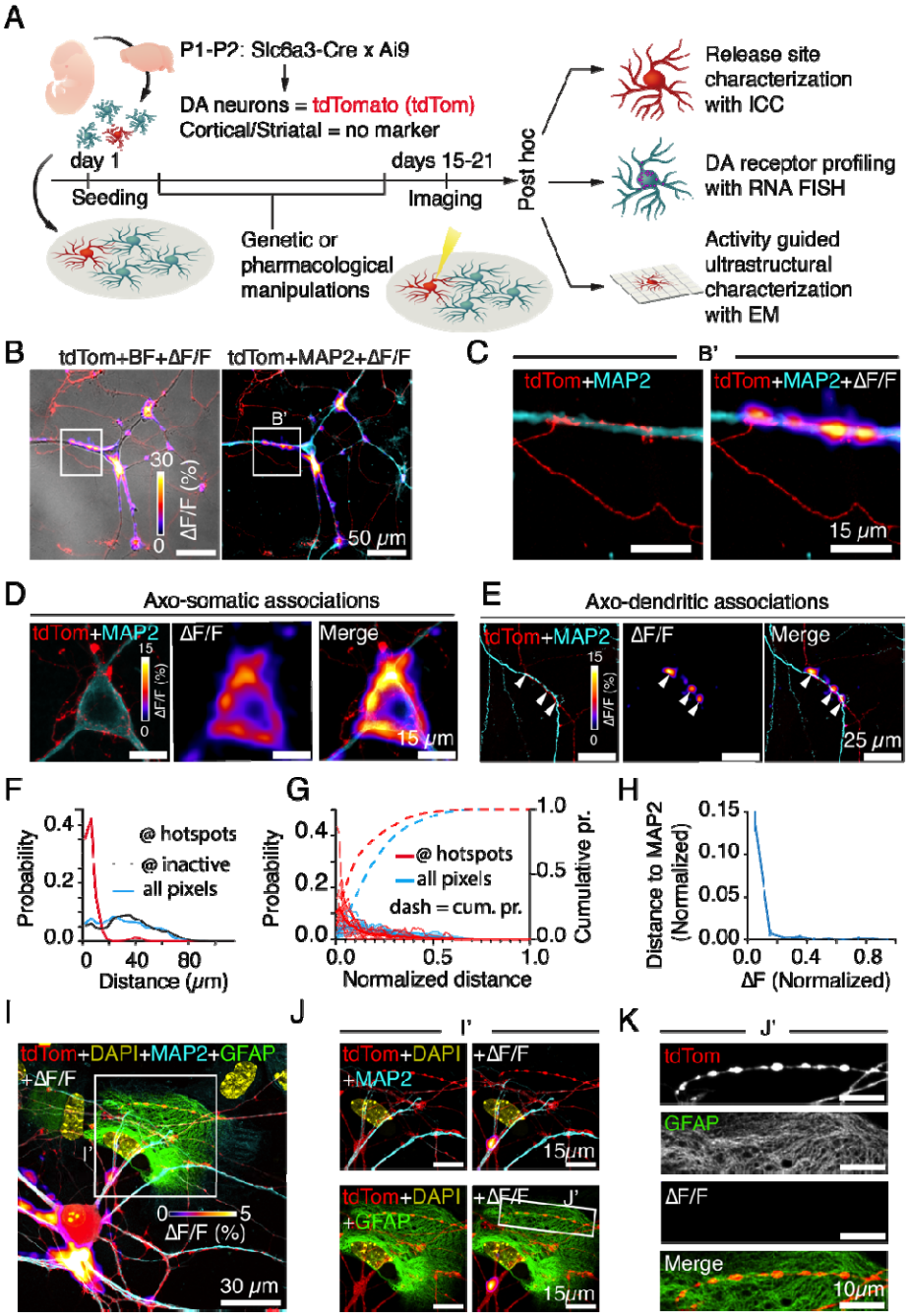

Fig. 1. Experimental schematics and DopaFilm activity imaging in axonal arbors of dopamine neurons.

(A) Experimental workflow. Dopamine neurons and striatal or cortical neurons are extracted from transgenic mice pups at P1-P2 and co-cultured on DopaFilm.

(B) An axonal arbor of a dopamine neuron expressing tdTomato (red, tdTom) in co-culture with a cortical neuron that is seen in brightfield (BF) image during live cell imaging. Evoked dopamine activity was captured by DopaFilm and overlaid with the BF and tdTom images (heat map). Right: confocal images of the same field of view (FOV) after post-hoc immunocytochemistry (ICC) against MAP2 (cyan).

(C) Close-up view of region of interest (ROI) (B', white box) depicted in (B) is shown. Note that the release capable tdTom+ varicosities are clustered near the dendrite (MAP2) and non-apposed varicosities do not release dopamine.

(D) An airyscan image of an axonal arbor of a dopamine neuron (tdTom) innervating a cortical neuron cell body (MAP2). FOV containing tdTom+MAP2, dopamine ΔF/F frame and merged images are shown.

(E) FOV consisting of an axonal process (tdTom) innervating a distal dendrite of a cortical neuron (MAP2). Note that dopamine varicosities release dopamine only when dendritically apposed (release hotspots are shown in white arrowheads).

(F) Clustering analysis: distribution function of pair-wise distances between tdTom pixels that overlap with ΔF hotspots (red), tdTom pixels that do not overlap with ΔF hotspots (black) and all tdTom pixels (blue). This data corresponds to image shown in Fig. 1B.

(G) Pooled clustering analysis. Red traces represent distribution of interpixel distances at release competent tdTom processes and blue traces represent overall interpixel distance distributions at all tdTom pixels. Each field of view of imaging contributes a red and a blue trace. Distances are normalized to enable direct comparison across FOVs of different sizes. Thick solid lines represent averages. Dash lines represent cumulative distribution functions (right y-axis).

(H) Proximity analysis: plot of normalized ΔF value at a tdTom pixel as a function of its distance from a MAP2+ pixel. Higher ΔF regions occur close to MAP2+ pixels. This data corresponds to image shown in Fig. 1B.

(I) FOV containing a tdTom positive dopamine neuron (soma and dendrites are in view) immunostained against MAP2 (cyan) and GFAP (green) and co-stained with nuclear stain DAPI (yellow).

(J) Enlarged view of ROI depicted in I (I', white box) with overlaid images of tdTom, DAPI, MAP2 and ΔF/F heatmap (top) and overlaid images of tdTom, DAPI, GFAP and ΔF/F heatmap (bottom). Note that dopamine release is evident at MAP2+ neuronal processes but not at GFAP+ glial processes.

(K) Enlarged view of ROI depicted in J (J', white box). tdTom, GFAP, ΔF/F and merged images are presented. The tdTom varicosities do not participate in release despite their proximity to glial processes.

We identified two types of associations between release competent dopamine neuron axons and their targets: those that were dendritically apposed (Fig. 1C, 1E), and those that are soma-apposed (Fig. 1D). Axo-somatic juxtapositions often presented as pericellular basket innervations (~74%, 39 out of 53 cortical neurons that received somatic dopamine input). These types of innervation have been described in some excitatory and inhibitory cell types(*39, 40*). In our assay, we found that these innervations were often sites of highly concentrated dopamine release (Fig. 1D, Animation 1, fig. S4 – S9). Importantly, inspection of dopamine secretion along the contours of individual axonal processes revealed that release competence is highly sensitive to proximity to and juxtaposition against other neuronal processes (Fig. 1C, 1E, fig. S2C – S2D, fig. S12, fig. S14)**.** Here, contiguous dopamine release events were observed at inter-hotspot distances of 11.2±5.4 µm (Mean±SD, n = 122 hotspots pooled from n = 17 samples), all localizing to MAP2-positive dendritic processes with which the dopaminergic axons were

associating. The inter-hotspot distances are consistent with the peak observed in pairwise distance distributions of release competent tdTom pixels (10.5±7.9 µm, Mean±SD). Notably, while proximity to neuronal processes strongly correlated with release competency, proximity to glial cells did not, and dopamine neurons maintained their preferred associations with neuronal processes even when glial processes were present (Fig. 1I – 1K, fig. S19). Taken together, our observations contradict the prevailing understanding that juxtaposition against target neurons is not a requirement for the release of neuromodulators like dopamine.

Moreover, dopamine release often exhibited an all-or-nothing characteristic, with active varicosities exhibiting a high probability of release (fig. S20A) whereas quiescent ones remained inactive. Dopamine release scaled with the strength of field stimulation (fig. S20B – S20C) and was abolished when extracellular calcium was removed (fig. S21), or when voltage-gated sodium channels were blocked using tetrodotoxin (TTX) (fig. S22), which are all characteristics commonly associated with neurochemicals secreted at synapses. Thus, we conclude that dopamine is predominantly released from axonal varicosities that are somehow associated with the dendrites and soma of putative target neurons, whereas processes that lacked juxtaposition had a strongly diminished probability of release.

Dopamine Releasing Varicosities are Enriched with Specializations that Facilitate Temporally Precise Neurotransmitter Release

We used immunofluorescence microscopy to assess presynaptic specialization in dopamine releasing varicosities (Fig. 2). In fast chemical synapses, the scaffolding protein bassoon (BSN) is enriched in the active zone and is one of the first proteins exported to axonal terminals during assembly of the presynapse(*41, 42*). We assayed the expression levels of BSN and several other key presynaptic proteins using immunofluorescence combined with confocal or airyscan imaging. Our findings show that BSN is a strong correlate of release competency in dopamine axonal varicosities (Fig. 2A). Expression levels of BSN correlated positively with the amplitude of ΔF (fig. S23). Notably, BSN was enriched at release sites, and its expression level was low in quiescent varicosities (Fig. 2A, fig. S23).

The correspondence between DopaFilm hotspots and BSN enriched varicosities was precise, especially at non-branching axons (Fig. 2A, Fig. 2B ROI-1 & ROI-2). However, clustering of varicosities occurs when axons contact dendritic shafts or at branching points (Fig. 2B ROI-3 & ROI-4). In such cases, clustered hotspots measured by DopaFilm lacked visually identifiable individual hotspots, but hotspots could still be computationally identified through non-negative matrix factorization (NNMF) analysis of the ΔF movie (see Methods for details) (fig. S24). The NNMF-delineated hotspots colocalized with individual BSN puncta or clusters of BSN puncta in immunofluorescence microscopy images (compare Fig. 2B, ROI-1 & ROI-2 vs. ROI-3 & ROI-4). In processes where DopaFilm hotspots can be precisely co-localized with varicosities, we used synaptophysin (SYP) immunofluorescence to show that these varicosities are enriched with synaptic vesicles, with the enrichment more prominent at the interface between varicosities and the dendrites they innervate (Fig. 2C). Examination of the vesicle priming protein MUNC13-1, and t-SNARE protein syntaxin 1, both essential for exocytotic neurotransmitter release, revealed their enrichment at dopamine release sites (fig. S25). The expression levels of the v-SNARE

protein synaptobrevin 2 (Vamp2) and the Ca^{2+} sensor synaptotagmin 1 (Syt1) similarly showed enrichment in release competent varicosities (Fig. 2D, fig. S26 – S27).

To determine if these typical constituents of presynaptic terminals are necessary for dopamine release, we used RNA interference mediated gene knockdown. Dopamine release was attenuated when we knocked down the expression levels of BSN, MUNC13-1, VAMP2, SYT1 and RIM1 using shRNA mediated gene silencing (Fig. 2E, Methods). In contrast, we did not observe any diminution in evoked and spontaneous dopamine release in cells transduced with control shRNA (scrambled sequences, Fig. 2E). We validated all knock down constructs in hippocampal cultures by probing corresponding RNA transcript levels using HCR RNA-FISH (fig. S28, Methods).

Furthermore, using immunofluorescence experiments, we discovered that the vesicle content of a varicosity is not a reliable indicator of its competency to release dopamine. We combined activity imaging with immunostaining for synaptophysin (SYP) or vesicular monoamine transporter 2 (VMAT2) to assess vesicle content. Our results showed that a considerable fraction of inactive varicosities contained vesicles, as shown by SYP immunostaining (fig. S29). Using VMAT2 staining, which is more specific to dopamine containing vesicles, we observed that up to ~48% of VMAT2 positive varicosities were quiescent (fig. S30). This observation strongly suggested that vesicle content is not a reliable proxy for dopamine release. We considered the possibility that some vesicle-containing varicosities might fail to release dopamine due to insufficient Ca^{2+} entry, which is necessary for exocytotic neurotransmitter release. To explore this, we probed subcellular Ca^{2+} dynamics using cre-dependent jGCaMP8 expression in dopaminergic processes while imaging dopamine release in the orthogonal NIR/SWIR channel where DopaFilm fluoresces (fig. S31A). Our investigation did not uncover differences in Ca^{2+} entry that corresponded to the variations in dopamine release, as robust Ca^{2+} signals were evident in all neuronal processes (fig. S31B – S31E). While it is possible that some release events may have fallen below DopaFilm's limit of detection, it is unlikely that all varicosities with Ca^{2+} entry participated in dopamine release. In conclusion, while dopamine-releasing varicosities exhibit presynaptic specializations akin to classical synapses, not all vesicle-containing varicosities possess cytomatrix proteins required for release competence. Therefore, caution should be exercised when using vesicle content as a proxy for release capability.

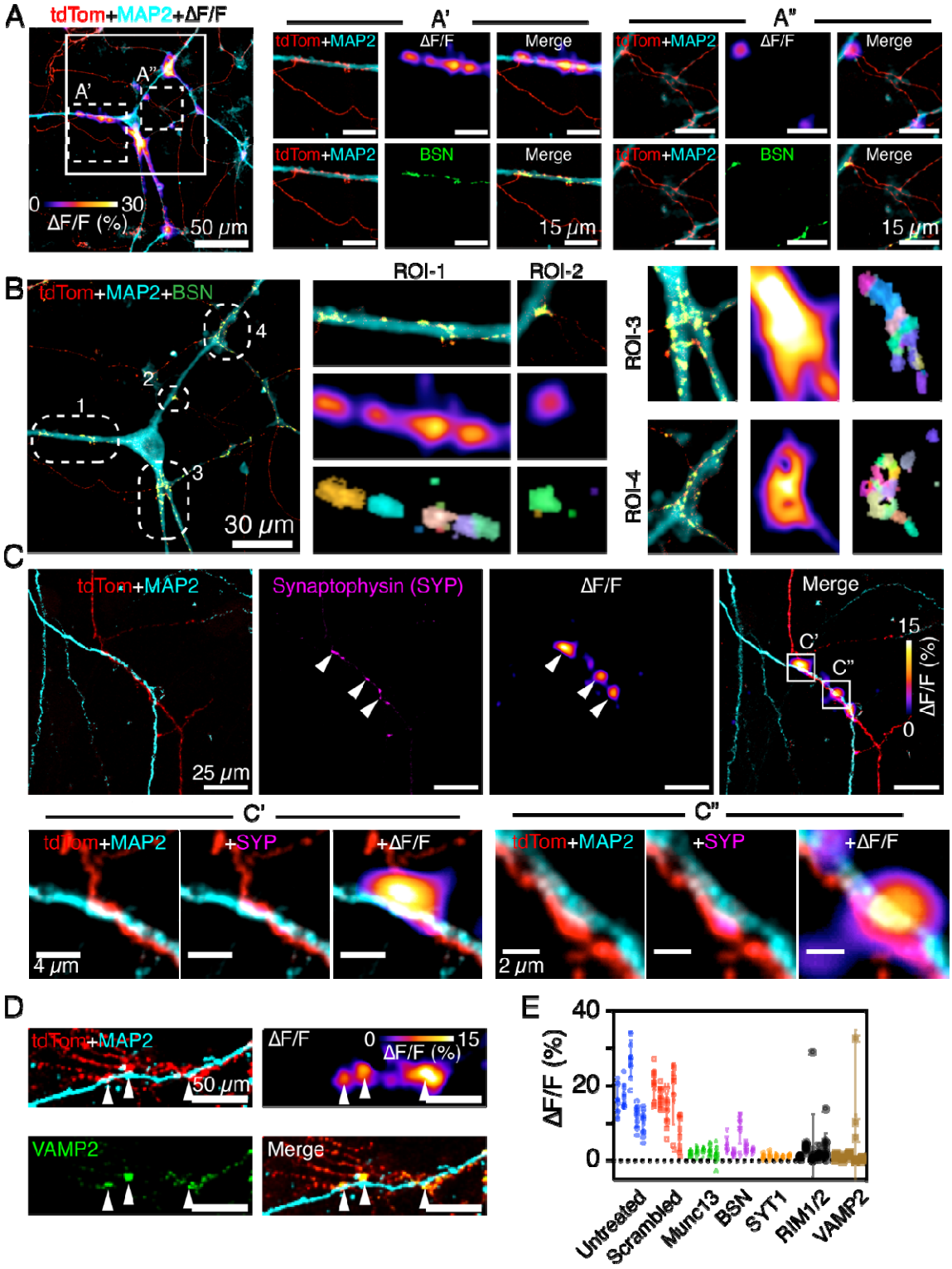

Fig. 2. Assessment of release machinery at dopamine releasing varicosities.

(A) Dopamine neuron axonal processes in red (tdTom) innervating a MAP2 immunostained cortical neuron in cyan, overlaid with dopamine release activity measured on DopaFilm (ΔF/F). Right: the regions shown in dashed white

boxes (A' and A") are expanded and overlaid with ΔF/F frames and bassoon (BSN) expression in green.

(B) Expanded FOV from the region shown in Fig. 2A (solid white box) overlaid with tdTom (red), MAP2 (cyan) and BSN (green). BSN-enriched varicosities appear as yellow. Panels on the right represent close-up view of ROIs 1– 4 (round white boxes with dashed lines). Each ROI panel shows a three-channel overlay of dopamine varicosities in red, bassoon in green, and dendritic processes in cyan, the corresponding dopamine release profile (ΔF/F) and hotspots computationally identified through NNMF (colored pixels). For ROIs 1-2 each hotspot identified in NNMF is spatially distinct and is assignable to single varicosities. For ROIs 3-4, the BSN-enriched dopaminergic varicosities are clustered. Although not visually apparent from the ΔF/F image, the clustered dopamine release hotspots can be computationally delineated into putative single release sites using NNMF (color coded pixels).

(C) Dopamine axonal process (tdTom) innervating a dendrite (MAP2), overlaid with dopamine release activity measured on DopaFilm (ΔF/F). Bottom row: close-up of ROI's C' and C" show that release competent varicosities are apposed against dendrites and are enriched in synaptophysin (SYP, magenta) at the interface between the red and cyan channels.

(D) Synaptobrevin 2 (VAMP2) is a strong corelate of dopamine release. Majority of the dopaminergic varicosities in this FOV are quiescent and the few active varicosities are enriched in VAMP2.

(E) shRNA mediated gene silencing of select presynaptic proteins leads to strongly diminished dopamine release. ΔF/F data from n=10 hotspots pooled from n=5 fields of view are presented. Treatment with scrambled sequence does not statistically differ from untreated sample (n.s.), whereas all other treatments do ($p < 10^{-4}$), all using Mann-Whitney test.

Ultrastructural Assessment of Dopamine Releasing Varicosities in Contact with Dendrites and Soma.

A significant source of uncertainty regarding the nature of dopamine release sites stems from the observation that the majority of vesicle-containing varicosities do not form classical synapses in immunofluorescence and EM-based ultrastructural studies(*10, 43-45*). However, the absence of correlated activity data in these studies leaves the functional role of non-synapse forming varicosities ambiguous. Moreover, the potential for neuromodulatory synapses to display morphological distinctions from classical synapses has largely been overlooked, making it risky to assess functionality based solely on ultrastructural ground truth established by ionotropic synapses.

Owing to the single bouton-level resolution offered by our assay, we took an unbiased approach to assess the ultrastructure of dopamine releasing sites by using correlated light (dopamine activity) and electron microscopy experiments (Fig. 3A). In co-cultures of midbrain dopamine neurons and cortical neurons, the predominant forms of innervations were onto soma and the proximal dendritic shafts that originate from the soma (70 neurons out of 86 cortical neurons). Dopaminergic varicosities targeted distal dendrites but did so less frequently (16 out of 86 neurons). Most of the dopamine releasing varicosities we examined near dendrites had clear small vesicles and formed symmetric synapses that showed little enhancement in electron density on the postsynapse (Fig. 3B – 3C, fig. S32). Notably, active varicosities that innervate distal dendrites formed synapses that resembled classical synapses in ultrastructure, with well-defined and rigidly parallel membranes at the cleft (Fig. 3B – 3C, fig. S32). On the other hand, dopamine releasing varicosities that target dendritic shafts and soma tended to exhibit diverse morphological characteristics with undulating (as opposed to parallel) membranes at the cleft, with the presynapse containing clear and pleomorphic vesicles that were sometimes loosely

clustered (Fig. 3D – 3E, fig. S33). Dense core vesicles were also evident in some release-competent varicosities (Fig. 3E). In summary, ultrastructural data shows that dopamine releasing varicosities share similarities with classical synapses, though they exhibit important morphological distinctions when compared to classical fast synapses.

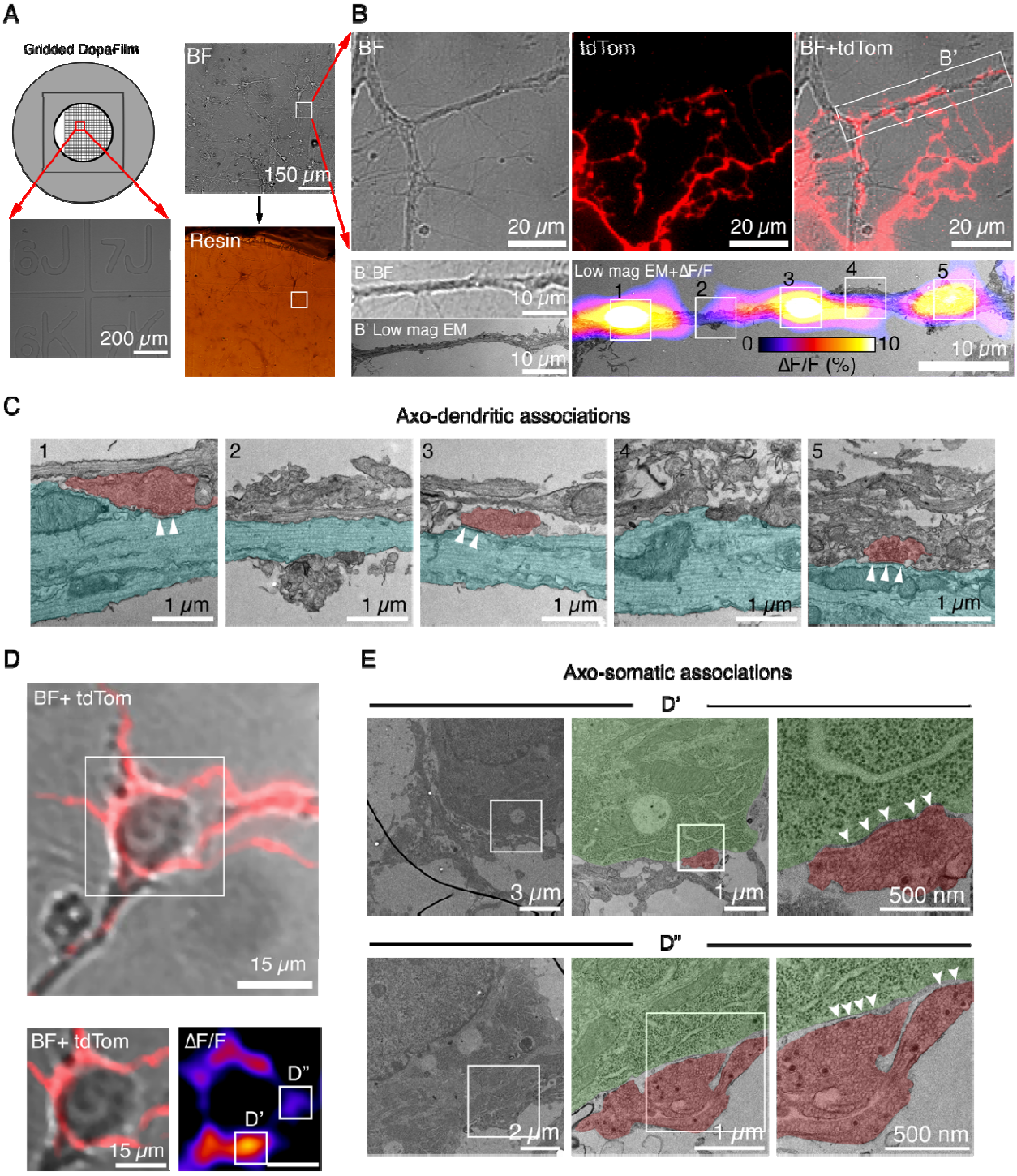

Fig. 3. Activity-guided ultrastructural characterization of dopamine release sites near dendrites and soma of target neurons.

(A) Schematic of a gridded (alphanumerically patterned) cell culture dish where sparse monolayers are co-cultured on DopaFilm. After dopamine release sites are recorded in live cell imaging, the specimen is fixed and processed for EM (Resin) (see Methods). The ROI is identified in the resin and trimmed. Thin serial sections collected from the resin blocks are imaged using TEM.

(B) Dopaminergic axonal processes innervating a dendrite of a cortical neuron from the ROI depicted with a white box in (A). Brightfield (BF), tdTom and overlaid images are shown in top panel. The bottom panel shows a close up of B' (white box) in BF, and the corresponding low magnification (Low mag) TEM images of B'. Also shown are DopaFilm hotspots mapped onto the low mag TEM image of B'.

(C) High magnification EM micrographs for white boxes 1 – 5 depicted in the bottom image panel of (B). The dendrite is given a cyan shade and dopaminergic varicosities are highlighted in red. Vesicle containing varicosities are evident at boxes 1,3 and 5 where dopamine release hotspot is present.

(D) Overlaid BF and tdTom images showing axonal innervation of the soma of a cortical neuron. Bottom panel: Zoomed-in images of BF+ tdTom and dopamine $\Delta F/F$ of the soma region.

(E) TEM micrographs of the soma showing D' and D" ROIs depicted in (D). Dopamine boutons (highlighted in red) are found juxtaposed against the soma (highlighted in green). Each image shows a zooms in on the regions outlined in solid white boxes.

Dopamine Axons Selectively Target Dopamine Receptor Expressing Neurons to form Synapses.

We investigated whether any post-synaptic specializations exist in the neuronal processes that are juxtaposed against release-competent varicosities (Fig. 4). Unlike the ubiquitously expressed receptors for fast ionotropic ligands, dopamine receptors are expected to be expressed in a cell-type specific manner in neurons. Axo-somatic associations observed between dopamine and cortical neuron co-cultures provide an ideal platform to address a fundamental question about the specificity of dopamine synapses. Specifically, we aimed to determine if axo-somatic innervations were established stochastically during axonal outgrowth or if dopamine neurons selectively targeted the subset of dopamine receptor expressing neurons in co-culture.

To explore the specificity of dopamine synapse formation, we performed gene expression profiling for dopamine receptors in putative target soma using post hoc RNA fluorescence in situ hybridization (FISH). Dopamine predominantly signals through D1 or D2 receptors, encoded by the Drd1 and Drd2 genes, respectively. We probed the expressions of these two transcripts using a modified RNAScope protocol (Methods). Our data show that dopamine neurons are highly selective in their innervation pattern in cortical co-cultures, predominantly targeting soma that express transcripts encoding for the Drd1 or Drd2 genes (Fig. 4A – 4C). To show this innervation pattern is not due to chance, we segmented all DAPI stained nuclei in a field of view innervated by dopaminergic axons, and computed distances between soma (putatively represented by DAPI pixels) and the nearest dopaminergic axonal process (i.e., tdTom pixels). We then plotted fraction of DAPI pixels as a function of their distances from tdTom pixels to show that Drd1-positive (Drd1+) nuclei are found closer to dopaminergic axons than is observed in the overall cellular population (Fig. 4D). Shuffling analysis showed that this pattern of innervation is unlikely to be due to chance (Fig. 4D). Similar innervation patterns and additional analysis are presented in later sections (see fig. S37, fig. S39–S40) and the results consistently indicate dopaminergic axons preferentially associate with cells that carry dopamine receptor transcripts.

In the preceding analysis, we used DAPI to “mark” the position of all cells in the field of view, but this did not differentiate between neurons and other cell types. Moreover, it did not rule out the possibility that dopaminergic axons might randomly release dopamine when contacting neuronal soma that lack dopamine receptors. To dig deeper, we focused on fields of view that contain dopaminergic axons that secrete an extracellular “corona” around a neuron, selectively targeting it over other nearby neuron(s). We then probed Drd1/2 transcript levels using RNAScope. Our findings are consistent with previous results: dopamine release was evident only in soma that had Drd1 or Drd2 transcripts (Fig. 4E – 4F). In contrast, axons that contacted neurons without Drd1/2 did not release any dopamine (Fig. 4F). This indicates that mere proximity to and juxtaposition against neuronal processes is not sufficient for dopamine release competency. Instead, dopamine axons innervate dopamine receptor expressing cells from the co-culture population, and that association then appears to facilitate release competency in these axons.

As we noted in preceding sections, axo-somatic innervations generate a dopamine release profile that appears as a “corona” around the target cell (Fig. 1D, Fig. 4C, fig. S4 – S9, fig. S25A – B). Soma that receive such dopamine fell into one of three categories: Drd1 expressing soma (8 out of 27 neurons), Drd1 and Drd2 co-expressing soma (8 out of 27 neurons) and Drd2 expressing soma (5 out of 27 neurons) (Fig. 4G – H, fig. S34). Previous reports have shown that dopamine’s effect in the prefrontal cortex and other cortical regions can be selectively abolished by D1 receptor antagonists and mimicked by D1 receptor agonists(*46-50*). This aligns with our observations, where dopamine axons tend to target and release onto Drd1-expressing cortical neurons in our co-culture setup. Interestingly, we also saw that some axo-somatic inputs went to neurons that did not seem to have Drd1 or Drd2 transcripts (6 out of 27 neurons) (fig. S34)**.** This could be due to low copy numbers of RNA transcripts that fell below the limit of detection of the FISH probes or because these neurons express other dopamine receptors subtypes (Drd3 – Drd5). Based on these data, we conclude that release-competent varicosities are paired up with processes that have the right transcriptomic profiles to express cognate receptors for dopamine.

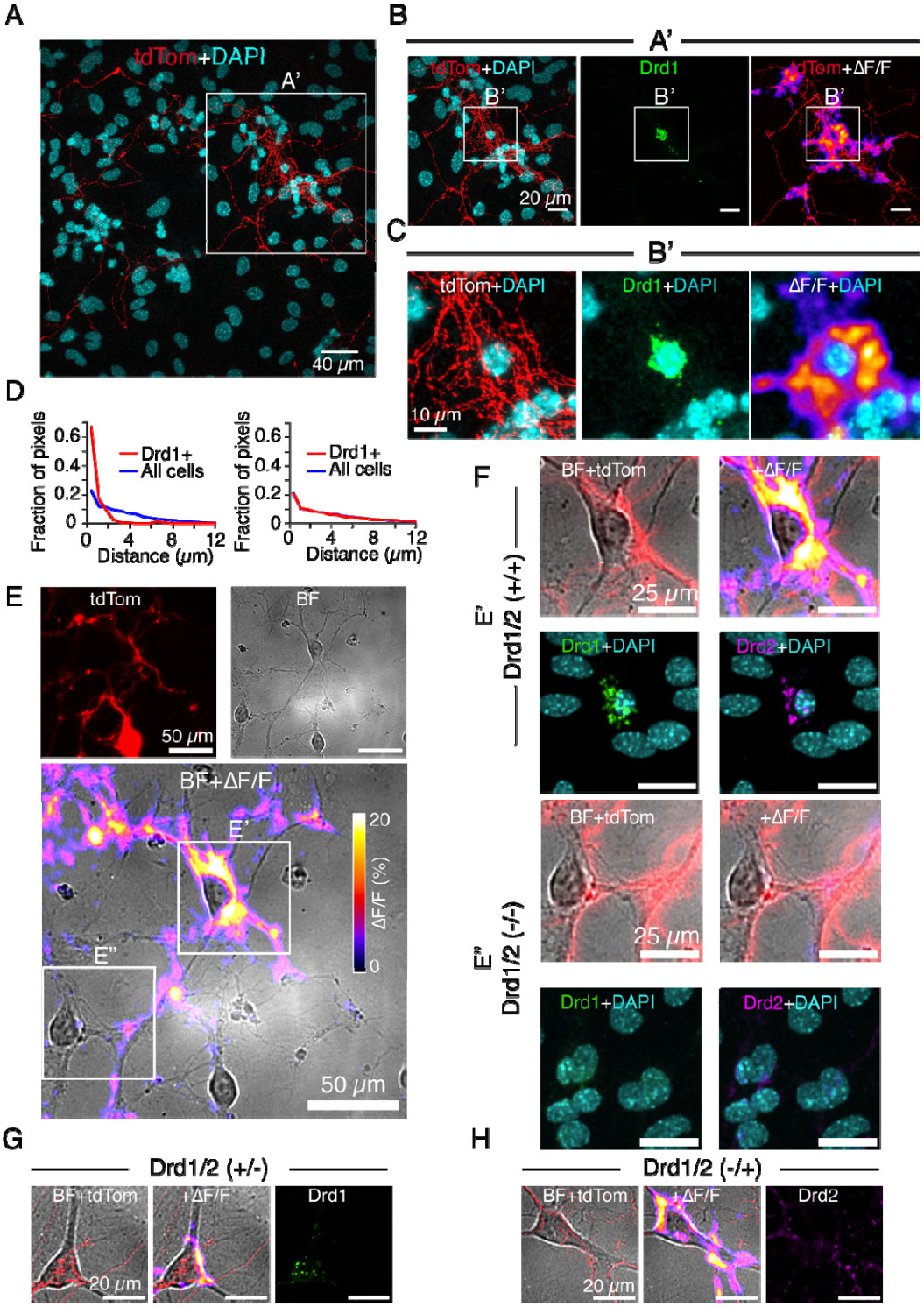

Fig. 4. Dopamine axons target dopamine receptor expressing neurons to form synapses.

(A) A FOV showing dopaminergic axonal processes (red) and DAPI stain (cyan). Note the convergence of dopamine axons towards the cell at the center of the solid white box (A').

(B) The white box (A') depicted in panel (A) is expanded and shown as a three-panel figure, including tdTom+DAPI, Drd1 signal from RNAScope, and tdTom+ΔF/F showing dopamine release. Note the convergence of tdTom processes towards the Drd1-positive soma, and the robust dopamine secretion around the soma.

(C) A close-up corresponding to the white box (B') depicted in (B), highlighting a "corona" of extracellular dopamine around the Drd1-positive soma.

(D) Distance transform analysis shows that convergence of dopamine axons onto Drd1-positive soma is unlikely to be due to chance. Fraction of DAPI+ pixels are plotted as a function their distance from nearest tdTom pixel. DAPI pixels from Drd1-positive cells (red) have a markedly different distribution compared to the overall distribution (blue). Nearly all of the Drd1-positive DAPI signal (97%) is found within 2 µm of a tdTom process vs. 56% for the overall population (blue); p-value $< 10^{-4}$ at 99% significance level on Drd1+ vs. all cells distribution using two sample Kolmogorov-Smirnov test, KS statistic = 0.918. Right: shuffling analysis shows the observed differences are not due to chance. tdTom pixels were randomly translated while DAPI pixels remained static, and the analysis was repeated over 100 such shuffling trials. The mean of the distributions from 100 trials shows no difference in the profile between Drd1-positive cells and all cells.

(E) A FOV of imaging showing an axonal arbor of a dopamine neuron (tdTom), and the corresponding brightfield image (BF). At the bottom is a bigger image of the same FOV with dopamine release (ΔF/F) and BF images shown as a merge. Note the cortical neuron soma depicted in E' receiving an extracellular "corona" of dopamine activity whereas the cortical neuron depicted in E" does not.

(F) Close up of E' and E" showing tdTom innervation, ΔF/F heatmaps, DAPI stain and readout from RNAScope. Neuron in E' is positive for both Drd1 and Drd2 whereas the neuron in E" is negative for both. Note the absence of dopamine release in E" despite some innervation by dopaminergic axons.

(G) A representative example of a Drd1 positive cortical neuron receiving dopamine input at the soma. This is the most frequently observed type of innervation in our experiments.

(H) A representative example of a Drd2 positive cortical neuron receiving dopamine input. This type of innervation is less frequently observed in our experiments.

The Postsynaptic Response Near Dopamine Release Site is Dopamine Release Gated and Spatiotemporally Precise

Fast chemical synapses evoke excitatory or inhibitory currents in their postsynaptic partners, and this prompted us to explore whether a biochemical equivalent exists in postsynaptic partners of dopamine synapses. Leveraging the high spatiotemporal resolution afforded by our assay and the spectral compatibility of the dopamine nanosensors with other genetically encoded probes, we measured changes in cyclic AMP (cAMP) levels that result from the activation of dopamine receptors. To assess baseline cAMP levels, first we measured cAMP levels at DIV 16 and DIV 21 in monocultures of cortical and striatal neurons using a genetically encoded fluorescence lifetime-based sensor, cAMPFire-L(*51*). At DIV16, cortical and striatal neurons had lifetimes of 2.50±0.09 ns and 2.58±0.12 ns (n=5, Mean ± SD) respectively, and at DIV21 lifetimes changed to 2.49±0.20 ns (-0.4% change relative to DIV16) and 2.38±0.12 ns (-8% change), respectively (fig. S35). Bath application of forskolin increased lifetimes by 35 – 37% at day 16 and ~22% at day 21 for cortical and striatal co-cultures, respectively (fig. S35). Next, we evaluated lifetimes in cortical or striatal neurons that were co-cultured with midbrain dopamine neurons. Compared to monocultures, baseline lifetimes decreased by ~ 8 – 9% for co-cultures at DIV16 (2.30±0.16 ns and 2.35±0.03 ns for cortical and striatal cocultures, respectively). However, lifetimes increased by ~10% for cortical neurons and ~20% for striatal at DIV21 (2.51±0.09 ns and

2.77±0.16 ns for cortical and striatal cocultures, respectively) (fig. S36). The increase in cAMPFire-L lifetimes from DIV16 to DIV21 in co-cultures is consistent with our observation where most of cell-autonomous dopamine neuron firing events are observed after DIV20. This data suggests that cAMP activity in striatal neurons is more robust than cortical neurons (fig. S36). Moreover, fluorescence lifetime-based quantification of cAMP levels highlight the influence of extracellular dopamine on neurons, suggesting the presence of functionally active dopamine receptors.

To get spatiotemporal information on dopamine release and cAMP modulations on target cells, we performed dual color imaging of dopamine and cAMP by the viral transduction of the intensity-based cAMP sensor G-Flamp1 in cortical and striatal co-cultures(*52*) (Fig. 5). We then examined the degree of colocalization between these two signals. Our findings suggest that cAMP activity in postsynaptic partners is spatiotemporally correlated with dopamine release, providing evidence for the functional integrity of dopamine synapses (Fig. 5A – C). Transcriptomic profiling using RNAscope showed that most cortical neurons that receive dopamine input express the D1 receptor (Fig. 4). As expected, we observed clear, dopamine receptor mediated increases in cAMP levels, with cAMP signal lagging dopamine signal by 4.3 ± 2.3 seconds (mean ± SD) (Fig. 5C, fig. S37). From axo-somatic dopamine input onto D2-expressing cortical neurons, we observed a temporally correlated decrease in cAMP across the soma and proximal dendrites (Fig. 5D – 5G). The receptor identity revealed by post hoc RNAScope readout was consistent with the direction of cAMP modulation (negative) measured by GFlamp1 (Fig. 5E). While cAMP activity in soma and major dendrites appeared to be highly synchronized and uniformly distributed (Fig. 5A, 5D, fig. S39 – S40), activity in distal dendritic processes showed localized hotspots that spatially correlated with the dopamine release heatmap recorded on DopaFilm (Fig. 5H, 5I).

In the volume transmission model of dopamine signaling, the spatial extent of signaling (i.e., "reach") from a release site is not fully understood, though some computational studies have made attempts to shed light on this process(*9, 53, 54*). Our findings so far suggest that dopamine signaling might be more spatially restricted, possibly confined to the spots where synaptic dopamine is released. To explore this further, we looked for cAMP modulations in neurons (both dendrites or soma) that were near dopamine release sites but were not directly synaptically connected. We observed that cAMP activity is strongly modulated at release sites but drops off significantly in areas where the dopamine only spills over (fig. S38 – S40). This shows that dopamine release hotspots trigger a biochemical response in target processes that matches the intensity of extracellular dopamine at those locations (Fig. 5H, fig. S38 – S40), revealing a spatially compartmentalized signaling than was previously underappreciated. This possibility is more compelling when considering the 2D nature of our assay, where dopamine spill over is less restricted compared to brain tissue. In summary, the evidence we have presented thus far points to a few key conclusions (1) dopamine is predominantly released from synapse-forming varicosities in axonal arbors, (2) the formation of these dopamine synapses is specific, likely molecularly guided rather than resulting from stochastic axonal outgrowth, and (3) dopamine synapses elicit a localized biochemical response in their postsynaptic partners, suggesting that the reach of dopamine signaling from a release site may be more limited than we think.

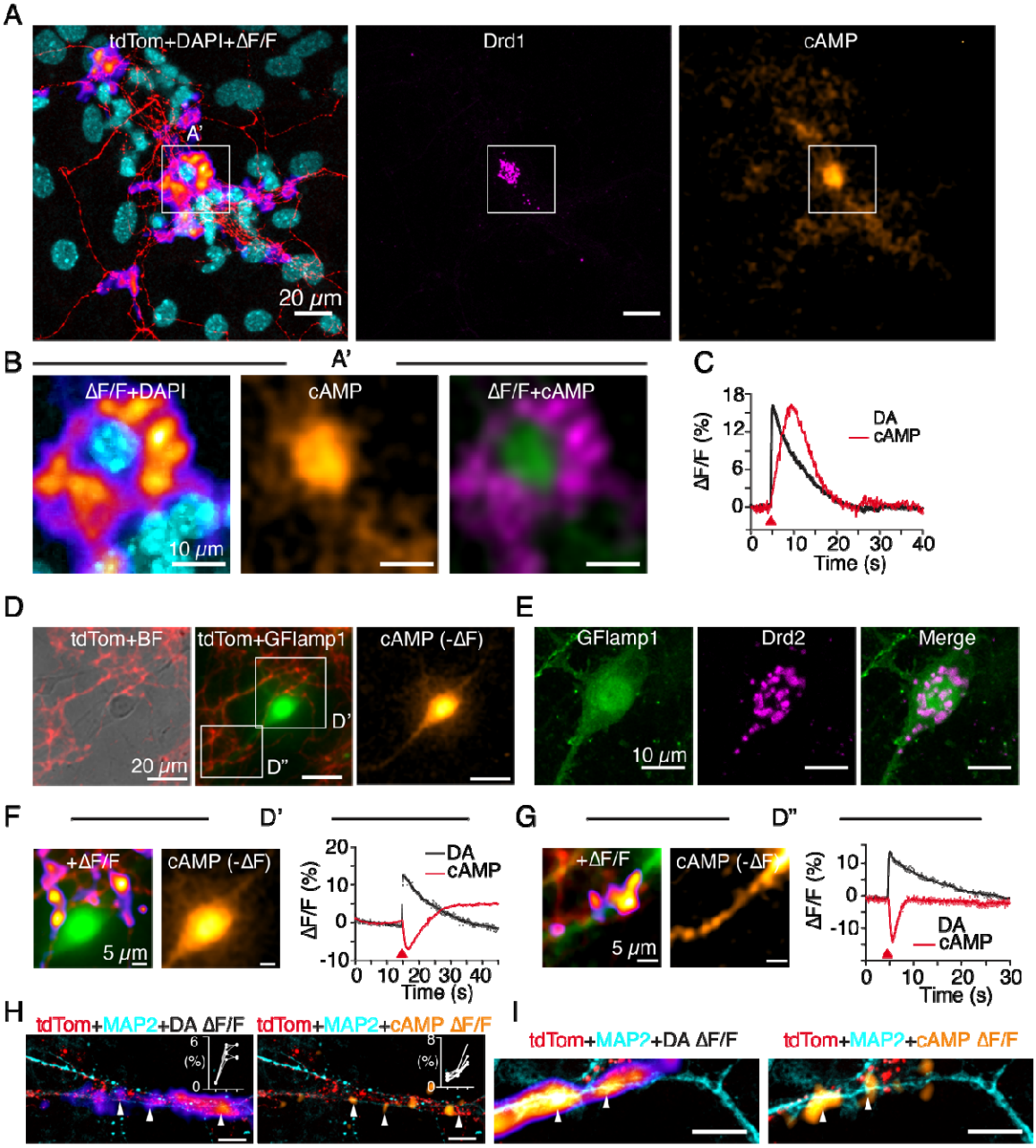

Fig. 5. Dopamine release rapidly modulates cAMP levels in target neurons.

(A) A three-panel figure showing tdTom, DAPI and ΔF/F, Drd1 RNA transcripts probed by RNAScope, and cAMP ΔF/F frame. Dopamine and cAMP ΔF/F images correspond to their respective peaks (see panel C), which occur at different time points after application of stimulus.

(B) Zoomed-in images of A' depicted in the solid white box in (A). Overlaid images of ΔF/F and DAPI, and cAMP ΔF frame (orange), and a merge of dopamine ΔF/F (magenta) and cAMP ΔF (green) are shown. An extracellular dopamine "corona" elicits a vigorous intercellular cAMP activity.

(C) Temporal traces of dopamine (black) and cAMP (red) for data shown in (B) are shown. Dopamine is presented as an average trace of identified hotspots and cAMP activity is averaged across the soma.

(D) A representative example of a dopaminergic axonal innervation of a cortical neuron exhibiting negative cAMP modulation at the soma and dendritic shafts. The cAMP pseudocolor is inverted for improved display. The neuron was confirmed to be positive for Drd2 transcripts using post hoc RNA FISH, as shown in (E).

(F,G) Zoomed-in images of white box ROIs depicted in (D), along with temporal traces showing dopamine and cAMP activity.

(H,I) cAMP activity hotpots generated by dopamine hotspots in distal dendritic processes in cortical neurons. Note that dopamine activity and cAMP activity are spatially colocated. Insets in (H): DA and cAMP peak ΔF/F scale with stimulation (2 pulses, 5 pulses and 10 pulses from left to right, all at 25 Hz).

Brain Slice Experiments Substantiate Key Findings of Co-Culture Assay

We sought to validate key findings from our co-culture assay through experiments conducted in brain slices. Midbrain dopamine neurons located in substantia nigra pars compacta (SNc) and ventral tegmental area (VTA) project their long-range axonal processes towards the striatum and various regions of the cortex (*55*). VTA projections to the prefrontal cortex (PFC) constitute part of the mesocorticolimbic system, responsible for dopamine's role in cognition and learning(*55*). Dopaminergic axonal projection density in the PFC is relatively sparse, and we asked if axo-somatic dopamine synapses, a key observation from co-culture experiments, could be observed in brain slices. To investigate this, we focused on two salient features of axo-somatic data: (1) clustering of varicosities around soma positive for Drd1 or Drd2 transcripts and (2) the enrichment of bassoon (BSN) within soma-innervating varicosities, which serve as a reliable indicator of release competency.

We prepared coronal brain slice sections from 3-month-old Slc6a3-Cre x Ai9 mice and immunostained them with the pan-neuronal marker NeuN and release-competency indicator bassoon (BSN) (Fig. 6A – 6B). We generated images from large fields of view in the PFC and used the image processing software Imaris to segment dopaminergic axonal varicosities into two subsets: those in contact with neuronal soma, representing release competent pericellular varicosities we observed in culture (shown in yellow, Fig. 6C), and those without such contact (shown in red, Fig. 6C). Notably, we found clusters of BSN enriched varicosities innervating a population of neuronal soma in the PFC (Fig. 6D, Animation 2). This subset comprised the majority of the varicosities detected (1737 out of 2400 varicosities, ~72%). In contrast, the varicosities that lacked contact with neuronal soma (28%) largely lacked BSN signal, indicating they were release incompetent, consistent with co-culture data (Fig. 6D, 6E). In soma-contacting varicosities, BSN signal was observed at the interface between the varicosities and NeuN-positive neurons (Fig. 6F). This observation aligns with the anticipated enrichment of BSN at the release-active interface (putative active zone of the varicosity). Notably, the vast majority (507 out of 636, ~80%) of soma that were innervated with clustered, BSN-positive varicosities were positive for Drd1, as detected using RNAScope (Fig. 6G). This finding is consistent with the propensity of dopamine axons for targeting Drd1-positive neurons in co-culture. These results demonstrate that key conclusions from our co-culture measurement can be corroborated in brain slice preparations.

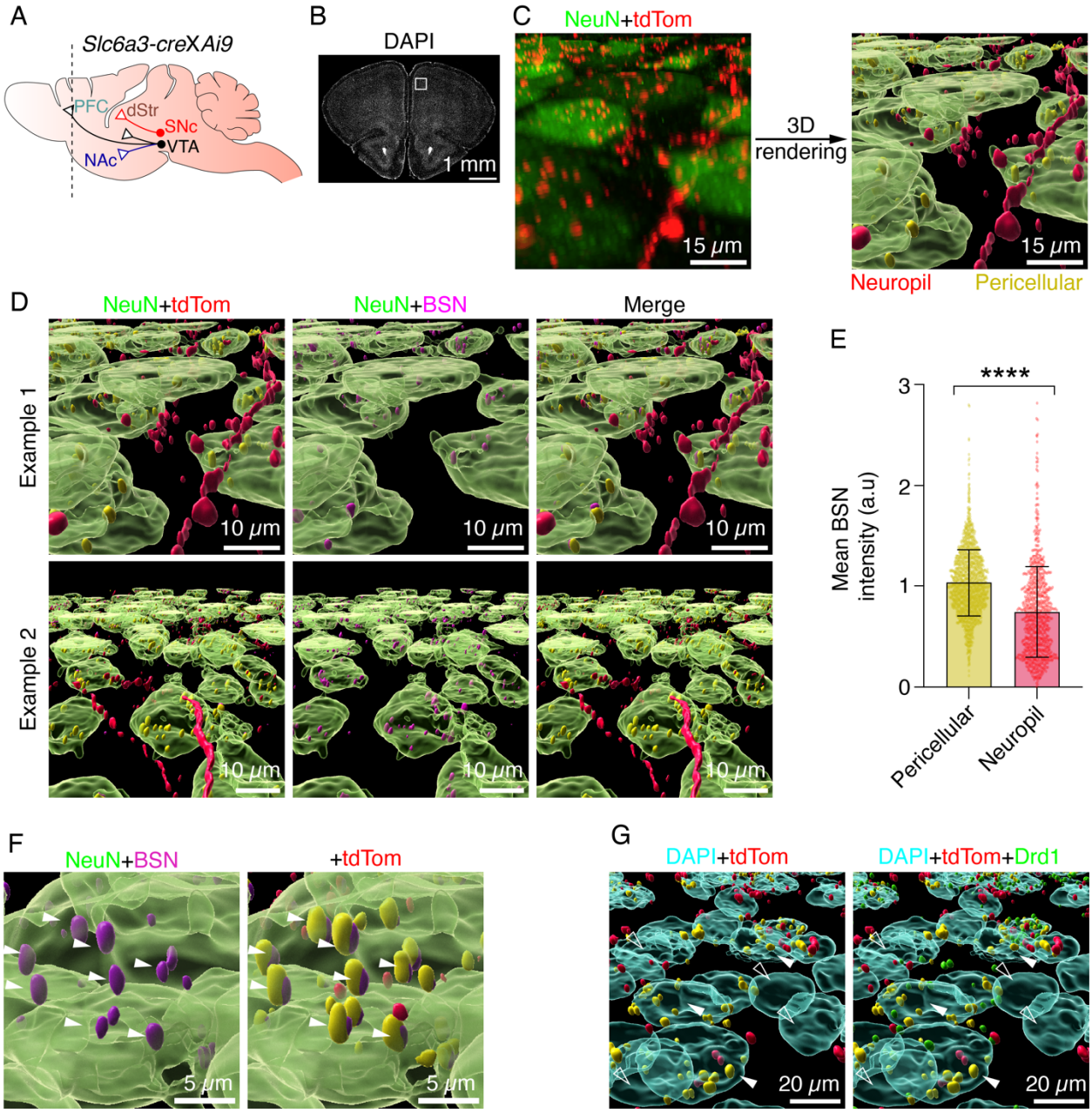

Fig. 6. Brain slice experiments substantiate key findings of co-culture assay.

(A) A sagittal cross section depicting dopamine neuron projections.

(B) A 50 µm coronal cross section (+2 mm from Bregma) was isolated from a fixed mouse brain followed by immunofluorescence microscopy and RNA FISH experiments.

(C) Confocal stacks for the ROI depicted in the white box in (B) were acquired for tdTom (red) and NeuN (green) channels. Image stack was stitched, deconvoluted, denoised and 3D reconstructions were carried out using Imaris image processing software. A FOV with the original confocal image and Imaris processed image is shown here for comparison. From the rendered image, dopaminergic varicosities are further classified into two: those that are in contact with soma (yellow, pericellular) vs those that are not (red, neuropil).

(D) Two examples showing overlaid images of NeuN (green), BSN (Purple) and tdTom (pericellular and neuropil) are presented. Note pericellular varicosities are enriched with BSN (yellow) and varicosities that are not in contact with soma (red) have relatively low expression of BSN.

(E) Mean BSN intensity as a function of varicosity classification (neuropil vs pericellular). BSN intensity in pericellular varicosities is higher than in the neuropil ($p < 10^{-4}$ using Kolmogorov-Smirnov test).

(F) The active zone (BSN signal)) in pericellular varicosities is oriented towards the soma. White arrowheads depict BSN enriched varicosities.

(G) An example of varicosities targeting Drd1 positive neurons in the prefrontal cortex. Overlaid images of tdTom (yellow and red), DAPI (cyan) and Drd1 (green) are shown here. Solid white arrowheads represent cells that are positive for Drd1, and these happen to be cells that are enriched in pericellular varicosities. Hollow arrowheads represent cells that are negative for Drd1, and these do not exhibit a clustering of dopamine varicosities.

Discussion: Our goal in this study was to address a key source of uncertainty in current investigations of dopamine release sites. Existing research in this area generally falls into one of two categories. The first category involves the use of immunofluorescence and electron microscopy to provide molecular and ultrastructural characterization of dopaminergic varicosities. These studies often lack functional activity data, leaving it unclear whether a varicosity containing vesicles or enriched in specific presynaptic proteins, but lacking synaptic juxtaposition, could participate in dopamine release(*28, 35, 56, 57*). On the other hand, in studies where extracellular dopamine dynamics is measured, this often involves the use of photometry or voltammetry probes that do not have single bouton resolution, making it difficult to map release activity from a varicosity to morphological, ultrastructural or molecular data(*32, 33, 35*) Our experimental workflow addresses these limitations through the subcellular visualization of dopamine release in dopaminergic axonal arbors that were sparsely cultured with putative target neurons.

A fundamental characteristics of volume transmission, the primary mode of neuromodulatory signaling in the brain, is its relatively imprecise one-to-many (1: n) communication. This process is thought to rely on passive diffusion of signaling molecules through three-dimensional tissue, where the signal competes against active clearance and enzymatic degradation. Unlike fast synaptic transmission, our knowledge on signal transduction mechanisms in volume transmission are not as well developed. Specifically, the spatiotemporal constraints of diffusion driven receptor activation, believed to occur tens to hundreds of micrometers away from non-synaptic release sites, are somewhat speculative. Understanding how such diffuse signaling contributes to precise neuronal computations, particularly in brain regions with dense axonal innervation and broadly expressed target receptors, remains a significant challenge. Consequently, despite our relatively solid grasp of GPCR-mediated signaling, the rules and mechanisms by which neuromodulators that are released into the extracellular space recruit and engage the GPCR signaling transduction for neuronal computation remains inadequately understood.

In this study, we present a model of dopamine neuromodulatory signaling that challenges some prevailing elements of volume transmission. Specifically, we propose that dopamine release and signaling has an underappreciated synaptic character that supports locally precise signaling. This precision is facilitated by varicosities that contain presynaptic specializations for *temporally*

precise dopamine release, and by their proximity to postsynaptic processes that are equipped with the molecular machinery necessary to generate *locally* precise biochemical response.

Moreover, we demonstrate that dopamine release is more efficient than previously thought. An important tenet of our current understanding of neuromodulation is that synaptic coupling is dispensable for neurochemical release. Dopamine neurons exhibit dense and highly arborized axonal projection systems(*58*) and previous studies have shown that most varicosities in these projection systems do not secrete dopamine, with release originating from a small subset of varicosities (often estimated at ~30%)(*35*, *57*, *59*). The molecular mechanisms governing release competency and the factors that delineate varicosities into active and quiescent subsets have remained elusive. A plausible model is that membrane mechanics may play a role in inducing the extensive "pearling" observed in dopamine axons(*60*). Our study then suggests that postsynaptic coupling is important for presynaptic release competency, indicating that only subset of the axonal "pearls" (i.e., varicosities) which are apposed to appropriate postsynaptic partners become release competent. Our study therefore offers an explanation for a question that had remained unaddressed: how are release competent dopamine varicosities specified? This specification appears to be governed by synaptic coupling to correct target partners. Furthermore, this work offers a more efficient and parsimonious model of neuromodulatory signaling compared to the incumbent model: dopamine is released only in locations where the postsynapse is tuned to respond optimally to the released molecules (Fig. 7). This is facilitated by the synapse-like associations observed at dopamine release sites.

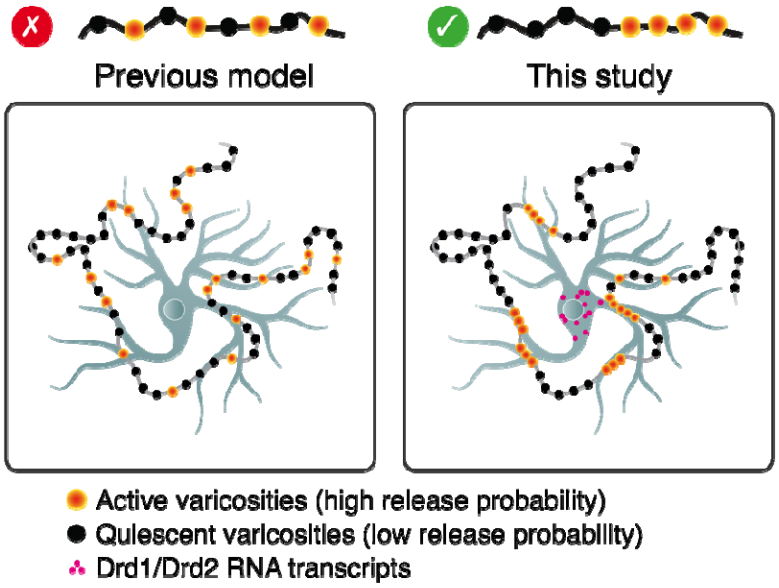

Fig. 7. A proposed model for dopamine neuromodulatory signaling.

Dopamine release sites exhibit a high degree of clustering. Clustered release sites are apposed to the dendrites and soma of neurons that express dopamine receptors. Release probability is low in varicosities that are not postsynaptically apposed.

The model of efficient neuromodulatory signaling we propose in this study is underpinned by the remarkable ability of dopamine axonal processes to accurately target their postsynaptic partners. Dopamine axons predominantly innervate the soma and proximal dendrites of their target cells, and despite the limited availability of dopamine receptor expressing cells in the co-culture assay, dopamine neurons demonstrate an impressive ability to converge their axonal processes towards the appropriate partners (Fig. 4A, fig. S39 – S40). Our findings emphasize a considerable wiring specificity in dopamine neurons that efficiently mobilizes the neuron's resources for optimal signaling by directing dopamine release towards the appropriate partners. We posit that clustered, multi-synaptic contact on individual soma helps maximize the influence of the released dopamine on the target cell, and hence efficient (Fig. 5A). The wiring specificity we observed is likely driven by molecular cues, the nature of which will be the subject of future studies. More importantly, several key observations made in brain slices substantiate our in vitro co-culture data on wiring specificity. First, in brain slices, we demonstrate that Drd1-positive neurons in the prefrontal cortex receive clusters of release competent boutons in a manner closely resembling our in vitro findings. Second, previous studies have showed that dopamine axonal projections into the basolateral amygdala target specific neuronal subpopulations, forming pericellular basket innervations that ensheath soma and proximal dendrites(*61-63*). Although these studies did not investigate dopamine receptor expression in target cells, the manner and density of innervation closely resemble our study's observations. Third, dopamine synapses have been observed to target GABAergic dendrites through a mechanism involving neuroligin-2(*29, 64*). Additionally, some EM studies have shown that most tyrosine hydroxylase immunoreactive boutons form symmetric synapses onto dendritic spines, shafts and soma of striatal neurons, clearly contradicting findings from other studies that show most boutons do not form synapses(*28*). While these studies did not directly visualize dopamine release and did not rule out release from non-synapse forming varicosities, they nevertheless provide additional evidence supporting the existence of molecular mechanisms that enable the formation and maintenance of dopamine synapses.

Does dopamine spill over from synapses contribute to neuromodulatory signaling? In our 2D culture system where the diffusive broadening of dopamine is minimally hindered, we see limited evidence of cAMP signaling mediated by dopamine spill over (fig. S38 – S40). This suggests that local hotspots of high dopamine release may be more efficient at activating dopamine receptors than a diffusing dopamine tone. This finding is consistent with previous studies conducted in brain slices, which have shown that a rapidly rising and high concentration of dopamine is necessary to elicit D2 receptor-induced GPCR-dependent potassium currents, also known as GIRK currents, in cell bodies of dopamine neurons(*65*). While our study does not entirely rule out diffusion mediated dopamine in activating peri-synaptic receptors, it nevertheless suggests that movement of dopamine through the interstitial fluid that fills the extracellular space is unlikely to be the primary mode of signaling. Thus, we conclude that dopamine release sites possess an underappreciated synaptic character that support spatiotemporally precise and efficient neuromodulatory signaling.

References and Notes

1. B. L. Sabatini, W. G. Regehr, Timing of synaptic transmission. *Annu Rev Physiol* **61**, 521-542 (1999).
2. Thomas C. Südhof, Neurotransmitter Release: The Last Millisecond in the Life of a Synaptic Vesicle. *Neuron* **80**, 675-690 (2013).
3. P. Greengard, The neurobiology of slow synaptic transmission. *Science* **294**, 1024-1030 (2001).
4. C. D. Grossman, J. Y. Cohen, Neuromodulation and Neurophysiology on the Timescale of Learning and Decision-Making. *Annual Review of Neuroscience* **45**, 317-337 (2022).
5. D. A. McCormick, D. B. Nestvogel, B. J. He, Neuromodulation of Brain State and Behavior. *Annual Review of Neuroscience* **43**, 391-415 (2020).
6. K. Fuxe *et al.*, The discovery of central monoamine neurons gave volume transmission to the wired brain. *Progress in Neurobiology* **90**, 82-100 (2010).
7. K. Fuxe *et al.*, From the Golgi–Cajal mapping to the transmitter-based characterization of the neuronal networks leading to two modes of brain communication: Wiring and volume transmission. *Brain Research Reviews* **55**, 17-54 (2007).
8. E. S. Vizi, A. Fekete, R. Karoly, A. Mike, Non-synaptic receptors and transporters involved in brain functions and targets of drug treatment. *British Journal of Pharmacology* **160**, 785-809 (2010).
9. M. E. Rice, S. J. Cragg, Dopamine spillover after quantal release: Rethinking dopamine transmission in the nigrostriatal pathway. *Brain Research Reviews* **58**, 303-313 (2008).
10. G. Wildenberg *et al.*, Partial connectomes of labeled dopaminergic circuits reveal non-synaptic communication and axonal remodeling after exposure to cocaine. *eLife* **10**, e71981 (2021).
11. V. M. Pickel, S. C. Beckley, T. H. Joh, D. J. Reis, Ultrastructural immunocytochemical localization of tyrosine hydroxylase in the neostriatum. *Brain Research* **225**, 373-385 (1981).
12. J. J. Bouyer, T. H. Joh, V. M. Pickel, Ultrastructural localization of tyrosine hydroxylase in rat nucleus accumbens. *Journal of Comparative Neurology* **227**, 92-103 (1984).
13. L. Descarries, O. Bosler, F. Berthelet, M. H. Des Rosiers, Dopaminergic nerve endings visualised by high-resolution autoradiography in adult rat neostriatum. *Nature* **284**, 620-622 (1980).
14. L. Stjärne, J. X. Bao, F. Gonon, M. Msghina, Nerve activity-dependent variations in clearance of released noradrenaline: regulatory roles for sympathetic neuromuscular transmission in rat tail artery. *Neuroscience* **60**, 1021-1038 (1994).
15. P. Séguéla, K. C. Watkins, L. Descarries, Ultrastructural relationships of serotonin axon terminals in the cerebral cortex of the adult rat. *J Comp Neurol* **289**, 129-142 (1989).
16. Z. Borosty¡nkői-Baldauf, Ultrastructure of Neuropeptide-Y Immunoreactive Elements in the Superior Colliculus of Cat. *Acta Biologica Hungarica* **53**, 23-31 (2002).
17. B. E. Maley, Ultrastructural identification of neuropeptides in the central nervous system. *J Electron Microsc Tech* **15**, 67-80 (1990).
18. L. Descarries, B. Alain, K. C. Watkins, Serotonin nerve terminals in adult rat neocortex. *Brain Research* **100**, 563-588 (1975).
19. J. F. Smiley, A. I. Levey, B. J. Ciliax, P. S. Goldman-Rakic, D1 dopamine receptor immunoreactivity in human and monkey cerebral cortex: predominant and extrasynaptic

localization in dendritic spines. *Proceedings of the National Academy of Sciences* **91**, 5720-5724 (1994).

20. P. Seeman, H. H. M. Van Tol, Dopamine receptor pharmacology. *Trends in Pharmacological Sciences* **15**, 264-270 (1994).

21. C. Missale, S. R. Nash, S. W. Robinson, M. Jaber, M. G. Caron, Dopamine Receptors: From Structure to Function. *Physiological Reviews* **78**, 189-225 (1998).

22. M. W. Howe, D. A. Dombeck, Rapid signalling in distinct dopaminergic axons during locomotion and reward. *Nature* **535**, 505-510 (2016).

23. J. A. da Silva, F. Tecuapetla, V. Paixão, R. M. Costa, Dopamine neuron activity before action initiation gates and invigorates future movements. *Nature* **554**, 244-248 (2018).

24. N. F. Parker *et al.*, Reward and choice encoding in terminals of midbrain dopamine neurons depends on striatal target. *Nature Neuroscience* **19**, 845-854 (2016).

25. L. T. Coddington, J. T. Dudman, The timing of action determines reward prediction signals in identified midbrain dopamine neurons. *Nature Neuroscience* **21**, 1563-1573 (2018).

26. J. E. Markowitz *et al.*, Spontaneous behaviour is structured by reinforcement without explicit reward. *Nature* **614**, 108-117 (2023).

27. V. Paget-Blanc *et al.*, A synaptomic analysis reveals dopamine hub synapses in the mouse striatum. *Nature Communications* **13**, 3102 (2022).

28. T. F. Freund, J. F. Powell, A. D. Smith, Tyrosine hydroxylase-immunoreactive boutons in synaptic contact with identified striatonigral neurons, with particular reference to dendritic spines. *Neuroscience* **13**, 1189-1215 (1984).

29. M. Uchigashima, T. Ohtsuka, K. Kobayashi, M. Watanabe, Dopamine synapse is a neuroligin-2-mediated contact between dopaminergic presynaptic and GABAergic postsynaptic structures. *Proc Natl Acad Sci U S A* **113**, 4206-4211 (2016).

30. K. K. L. Yung *et al.*, Immunocytochemical localization of D1 and D2 dopamine receptors in the basal ganglia of the rat: Light and electron microscopy. *Neuroscience* **65**, 709-730 (1995).

31. A. G. Beyene *et al.*, Imaging striatal dopamine release using a nongenetically encoded near infrared fluorescent catecholamine nanosensor. *Science Advances* **5**, eaaw3108.

32. F. Sun *et al.*, A Genetically Encoded Fluorescent Sensor Enables Rapid and Specific Detection of Dopamine in Flies, Fish, and Mice. *Cell* **174**, 481-496.e419 (2018).

33. T. Patriarchi *et al.*, Ultrafast neuronal imaging of dopamine dynamics with designed genetically encoded sensors. *Science* **360**, eaat4422 (2018).

34. B. G. Robinson *et al.*, RIM is essential for stimulated but not spontaneous somatodendritic dopamine release in the midbrain. *eLife* **8**, e47972 (2019).

35. C. Liu, L. Kershberg, J. Wang, S. Schneeberger, P. S. Kaeser, Dopamine Secretion Is Mediated by Sparse Active Zone-like Release Sites. *Cell* **172**, 706-718.e715 (2018).

36. C. Bulumulla *et al.*, Visualizing synaptic dopamine efflux with a 2D composite nanofilm. *eLife* **11**, e78773 (2022).

37. X. Zhuang, J. Masson, J. A. Gingrich, S. Rayport, R. Hen, Targeted gene expression in dopamine and serotonin neurons of the mouse brain. *Journal of Neuroscience Methods* **143**, 27-32 (2005).

38. S. Lammel *et al.*, Diversity of transgenic mouse models for selective targeting of midbrain dopamine neurons. *Neuron* **85**, 429-438 (2015).

39. A. Riedel *et al.*, Vesicular glutamate transporter 3-immunoreactive pericellular baskets ensheath a distinct population of neurons in the lateral septum. *Journal of Chemical Neuroanatomy* **36**, 177-190 (2008).
40. R. A. Senft, S. M. Dymecki, Neuronal pericellular baskets: neurotransmitter convergence and regulation of network excitability. *Trends in Neurosciences* **44**, 915-924 (2021).
41. S. R. Krueger, A. Kolar, R. M. Fitzsimonds, The Presynaptic Release Apparatus Is Functional in the Absence of Dendritic Contact and Highly Mobile within Isolated Axons. *Neuron* **40**, 945-957 (2003).
42. M. Shapira *et al.*, Unitary Assembly of Presynaptic Active Zones from Piccolo-Bassoon Transport Vesicles. *Neuron* **38**, 237-252 (2003).
43. C. Ducrot *et al.*, Dopaminergic neurons establish a distinctive axonal arbor with a majority of non-synaptic terminals. *The FASEB Journal* **35**, e21791 (2021).
44. L. Descarries, N. Mechawar, in *Progress in Brain Research*. (Elsevier, 2000), vol. 125, pp. 27-47.
45. L. Descarries, K. C. Watkins, S. Garcia, O. Bosler, G. Doucet, Dual character, asynaptic and synaptic, of the dopamine innervation in adult rat neostriatum: A quantitative autoradiographic and immunocytochemical analysis. *Journal of Comparative Neurology* **375**, 167-186 (1996).
46. L. Chen, J. D. Bohanick, M. Nishihara, J. K. Seamans, C. R. Yang, Dopamine D1/5 Receptor-Mediated Long-Term Potentiation of Intrinsic Excitability in Rat Prefrontal Cortical Neurons: Ca2+-Dependent Intracellular Signaling. *Journal of Neurophysiology* **97**, 2448-2464 (2007).
47. W.-J. Gao, L. S. Krimer, P. S. Goldman-Rakic, Presynaptic regulation of recurrent excitation by D1 receptors in prefrontal circuits. *Proceedings of the National Academy of Sciences* **98**, 295-300 (2001).
48. W. J. Gao, P. S. Goldman-Rakic, Selective modulation of excitatory and inhibitory microcircuits by dopamine. *Proc Natl Acad Sci U S A* **100**, 2836-2841 (2003).
49. A. Lavin, A. A. Grace, Stimulation of D1-type dopamine receptors enhances excitability in prefrontal cortical pyramidal neurons in a state-dependent manner. *Neuroscience* **104**, 335-346 (2001).
50. G. Witkowski, B. Szulczyk, R. Rola, P. Szulczyk, D1 dopaminergic control of G protein–dependent inward rectifier K+ (GIRK)–like channel current in pyramidal neurons of the medial prefrontal cortex. *Neuroscience* **155**, 53-63 (2008).
51. C. I. Massengill *et al.*, Sensitive genetically encoded sensors for population and subcellular imaging of cAMP in vivo. *Nature Methods* **19**, 1461-1471 (2022).
52. L. Wang *et al.*, A high-performance genetically encoded fluorescent indicator for in vivo cAMP imaging. *Nature Communications* **13**, 5363 (2022).
53. J. K. Dreyer, K. F. Herrik, R. W. Berg, J. D. Hounsgaard, Influence of phasic and tonic dopamine release on receptor activation. *J Neurosci* **30**, 14273-14283 (2010).
54. A. G. Beyene, I. R. McFarlane, R. L. Pinals, M. P. Landry, Stochastic Simulation of Dopamine Neuromodulation for Implementation of Fluorescent Neurochemical Probes in the Striatal Extracellular Space. *ACS Chemical Neuroscience* **8**, 2275-2289 (2017).
55. R. Y. Moore, F. E. Bloom, Central Catecholamine Neuron Systems: Anatomy and Physiology of the Dopamine Systems. *Annual Review of Neuroscience* **1**, 129-169 (1978).

56. L. Kershberg, A. Banerjee, P. S. Kaeser, Protein composition of axonal dopamine release sites in the striatum. *eLife* **11**, e83018 (2022).
57. A. Banerjee *et al.*, Molecular and functional architecture of striatal dopamine release sites. *Neuron* **110**, 248-265.e249 (2022).
58. W. Matsuda *et al.*, Single nigrostriatal dopaminergic neurons form widely spread and highly dense axonal arborizations in the neostriatum. *J Neurosci* **29**, 444-453 (2009).
59. D. B. Pereira *et al.*, Fluorescent false neurotransmitter reveals functionally silent dopamine vesicle clusters in the striatum. *Nature Neuroscience* **19**, 578-586 (2016).
60. J. M. Griswold *et al.*, Membrane mechanics dictate axonal morphology and function. *bioRxiv*, 2023.2007.2020.549958 (2023).
61. M. Brinley-Reed, A. J. McDonald, Evidence that dopaminergic axons provide a dense innervation of specific neuronal subpopulations in the rat basolateral amygdala. *Brain Research* **850**, 127-135 (1999).
62. O. Lindvall, Mecencephalic dopaminergic afferents to the lateral septal nucleus of the rat. *Brain Research* **87**, 89-95 (1975).
63. E. Asan, The catecholaminergic innervation of the rat amygdala. *Adv Anat Embryol Cell Biol* **142**, 1-118 (1998).
64. H.-J. Kim *et al.*, GABAergic-like dopamine synapses in the brain. *Cell Reports* **42**, 113239 (2023).
65. C. P. Ford, P. E. M. Phillips, J. T. Williams, The Time Course of Dopamine Transmission in the Ventral Tegmental Area. *The Journal of Neuroscience* **29**, 13344 (2009).

Acknowledgments: We would like to thank Phuong Nguyen for helping with primary culture requests; Morgan Clarke, Monique Copeland and Benjamin Foster for assistance with histology work, FISH and antibody screening tests. We would like to thank Janelia Viral Tools (Hyun Ah Yi) with packaging viruses and Janelia Molecular Biology team for help with plasmid preparations. We would like to thank Jeremy Hasseman for providing Syn-Flex-jGCaMP8m-WPRE virus. We would like to extend our gratitude to Dr. Gary Miller (Columbia University) for the rabbit anti-VMAT2 antibody. We would like to thank Eric Schreiter, Alison Tebo and Tim Brown for discussions related to cAMP imaging. We would like to thank Marla Feller and Bernardo Sabatini for helpful feedback on the manuscript. We would like to thank Kaspar Podgorski for sharing with us the analysis pipeline framework we used to analyze live-cell imaging data. **Funding:** This work was funded in full by the Howard Hughes Medical Institute.
Author Contributions: C.B and A.G.B designed the study and performed most imaging experiments. C.B and A.G.B carried out most of the data analysis, produced the figures and wrote the manuscript with assistance from the rest of the authors. D.W carried out the primary neuronal culture experiments with assistance from C.B. N.I performed most of the electron microscopy experiments with assistance from C.B. M.C and M.E assisted with FISH probe design and experiments. R.P assisted with FLIM experiments. D.Alcor assisted with tissue imaging and analysis. D.Ackerman developed most of the image analysis pipeline with assistance from A.G.B. Authors declare that they have no competing interests.

Supplementary Materials:

Materials and Methods
References
Figs. S1 to S40
Animation 1 to 2